Grant NsG - 405/14 - 007 - 003

ESTABLISHMENT OF THERMODYNAMIC AND TRANSPORT PROPERTIES FOR PARA-HYDROGEN

Final Report

September 1, 1963 - August 31, 1967

The original duration of this grant was two years from September 1, 1963 to August 31, 1965. However, the lack of graduate student assistance and the delay in the procurement of experimental viscosity and thermal conductivity data on para-hydrogen from the National Bureau of Standards at Boulder, Colorado necessitated the extension of this grant to August 31, 1967.

During this period, published experimental information and particularly that of the National Bureau of Standards was utilized to construct reduced density plots for para-hydrogen. This information with the atmospheric pressure heat capacity line permitted the establishment of enthalpy and entropy charts for this substance.

The only available experimental viscosity data for para-hydrogen, obtained by the National Bureau of Standards at Boulder, Colorado (10) was utilized to produce a reduced viscosity correlation for the gaseous and liquid states at cryogenic conditions. This correlation in conjunction with information available for normal hydrogen was then used to generate a reduced viscosity correlation applicable to higher temperatures and pressures.

Since experimental thermal conductivities for para-hydrogen in the dense gaseous and liquid states are not yet available, it became necessary to attempt the prediction of this transport property using the theoretical

approach of Enskog. In conjunction with this, the viscosity and self-diffusivity behavior were also estimated.

THERMODYNAMIC PROPERTIES OF PARA-HYDROGEN

The extensive experimental PVT studies of the National Bureau of Standards include data for the saturated vapor and liquid densities (22), freezing liquid densities (15), and the comprehensive superheated densities up to temperatures of 100°K and pressures of 350 atm (14).

In this investigation the following physical constants for p-hydrogen have been accepted:

Critical Point (22): $T_c = 32.976 \pm 0.015$°K

$P_c = 12.759 \pm 0.028$ atm

$\rho_c = 00001559 \pm 0.00005$ g-moles/cm^3

Normal Boiling Point (16,28): $T_b = 20.268$°K

Triple Point (16,22): $T_t = 13.803$°K $P_t = 52.8$ mm Hg

Molecular Weight (22): $M = 2.01572$

The PVT information has been utilized to construct the reduced density correlation presented in Figures 1 and 2. Figure 1 utilizes rectilinear coordinates and is more convenient for representing the high density region, whereas Figure 2 best represents this properly in the low density region.

The thermal data used include the experimental measurements for the heat capacity of the saturated solid (5,17,20), the heat of fusion at the triple point (29), the heat capacity of the saturated liquid (30), and the calculated heat capacity at constant pressure of gaseous p-hydrogen at 1 atm (23). Latent heats of vaporization, λ, were calculated (7) for p-hydrogen from the triple point to the critical point from the Clapeyron equation using the available vapor pressure data (1,16,28) and saturated density measurements (22).

The effect of pressure on the enthalpy and entropy follows from conventional thermodynamic relationships to be as follows:

$$\Delta H = -\int_{P_0}^{P}\left[\frac{1}{\rho} + \frac{T}{\rho^2}\left(\frac{\partial \rho}{\partial T}\right)_P\right] dP \qquad (1)$$

and

$$\Delta S = \int_{P_0}^{P} \frac{1}{\rho^2}\left(\frac{\partial \rho}{\partial T}\right)_P dP \qquad (2)$$

To calculate the necessary partial derivative, $(\partial \rho/\partial T)_P$, the isobars of Figures 1 and 2 were numerically differentiated by fitting a second degree orthogonal polynomial through a set of five points, the point of interest being the central point of the set.

The reference state was selected to be the solid state at T = 0°K where S = 0 Btu/lb °R and $H-H_0^\circ$ = 0 Btu/lb. For these thermodynamic calculations, experimental vapor pressures (22) were used to calculate latent heats of vaporization. In this regard, the constants of the Frost-Kalkwarf vapor pressure equation (13) were established to define the vapor pressure behavior of para-hydrogen between the triple point and the critical point as follows:

$$\ln P = 10.4791 - \frac{105.651}{T} + 0.425173 \ln T + 0.047310 \frac{P}{T^2} \qquad (3)$$

where P is the vapor pressure in millimeters of mercury and T represents the absolute temperature in degrees Kelvin. Details concerning the establishment of these constants and the latent heats of vaporization over the complete liquid range can be found elsewhere (9). The details of the required calculations for enthalpy and entropy can be found elsewhere (8). The final enthalpy and entropy plots for solid, liquid, and gaseous para-hydrogen are presented in Figures 3 and 4, respectively.

TRANSPORT PROPERTIES

The viscosity measurements on para-hydrogen reported by Diller (10)

were used as the basis for developing a reduced state viscosity correlation for this substance. Diller presents experimental viscosities for the gaseous and liquid states from 15°K to 100°K and pressures from 4.2 to 350 atm. In order to establish the temperature dependence of μ^*, the viscosity of para-hydrogen in the gaseous state at 1 atm., the isothermal data of Diller were extrapolated to $\rho = 0$. The intercepts represent μ^* and were found to be as follows:

T, °K	33	36	40	50	60	70	80	100
$\mu^* \times 10^5$, cp	172	184	203	247	285	324	355	420

These values can be expressed analytically in terms of reduced temperature as follows:

$$\mu^* \times 10^5 = 192.0\, T_R - 21.6\, T_R^2 + 1.28\, T_R^3 \qquad \text{for } T_R \leq 3.00 \qquad (4)$$

Values obtained from Equation (4) were in good agreement with the 1 atm viscosity measurements between 20.5°K and 77.8°K reported by Coremans et al (6). In their experimental study, no specific mention is made concerning the form of gaseous hydrogen used.

To examine differences in the μ^* versus T_R relationships between normal and para-hydrogen, values of μ^* obtained from the compilation of Stiel and Thodos (26) for normal hydrogen were used in conjunction with values obtained from Equation (4) for para-hydrogen to produce at the same reduced temperatures a linear plot of μ_p versus μ_n on log-log coordinates. This relationship can be expressed as

$$\mu_p^* = 1.004\, \mu_n^{*1.0029} \qquad (5)$$

For normal hydrogen, the value $T_c = 33.3$°K was used (19). Equation (5) was used to extend the μ^* values obtained from the work of Diller (10) to temperatures below 33°K.

An attempt to relate the residual viscosity, $\mu-\mu^*$, with ρ_R, the reduced density, using the viscosity values of Diller (10) has shown that individual relationships result for each temperature as shown in Figure 5. This temperature dependence is contrary to that encountered in the behavior of the dense gaseous and liquid states of such substances as argon (25), nitrogen (3), and carbon dioxide (18). For these substances unique relationships of $\mu-\mu^*$ versus ρ_R resulted which were independent of temperature. The anomolous behavior of para-hydrogen can be attributed to the excessive quantum deviations present in this substance which is very closely related to normal hydrogen, as indicated by Equation (5).

Figure 5 has proved useful in establishing the viscosity of para-hydrogen at the critical point. This was accomplished by extending the critical isotherm to $\rho_R = 1.00$, and thus establishing a value of $(\mu-\mu^*)_c = 182 \times 10^{-5}$ cp which corresponds to a value for the critical viscosity of $\mu_c = 354.5 \times 10^{-5}$ cp which was adopted in the subsequent development of a reduced viscosity correlation. This value of the critical viscosity agrees closely with that estimated by Diller (10), $\mu_c = (355 \pm 5) \times 10^{-5}$ cp.

Since Diller's work (10) does not include experimental viscosities for the saturated vapor, the experimental viscosities for the saturated liquid were used to obtain this information. A plot of $\mu-\mu^*$ versus ρ_R for the saturated liquid state was extended to the origin and this extension was assumed to describe the viscosity behavior of the saturated vapor. This analysis allowed the establishment of the complete saturated viscosity envelope.

All of the above information was then used to construct the reduced viscosity correlation for para-hydrogen presented in Figure 6. In order to provide a unified correlation for both normal and para-hydrogen, the

temperature range of Figure 6 was extended to $T_R = 100$. This was accomplished by accepting the viscosities for gaseous n-hydrogen at 1 atm above $T_R = 3.0$ reported by Stiel and Thodos (26). The viscosities in the high temperature region are consistent with those reported by Vanderslice et al (27) which resulted from molecular beam measurements. For normal hydrogen, the critical constants recommended by Kobe and Lynn (19) were adopted and are as follows: $T_c = 33.3°K$, $P_c = 12.8$ atm, and $\rho_c = 0.0310$ g/cm^3. For normal hydrogen, a critical viscosity of $\mu_c = 361.5 \times 10^{-5}$ cp makes the μ^* values reported by Stiel and Thodos (26) consistent with Figure 6 in the temperature interval $1.0 < T_R < 3.0$. Figure 7 represents the final correlation for reduced viscosity of gaseous and liquid normal and para-hydrogen for temperatures up to $T_R = 100$ and pressures up to $P_R = 30$.

PREDICTION OF PRESSURE DEPENDENCE ON TRANSPORT PROPERTIES

The effect of pressure on the transport properties of gases has been predicted by Enskog (12) and is described by the following relationships:

$$\frac{\mu}{\mu^*} = b\rho\left[\frac{1}{b\rho\chi} + \frac{4}{5} + 0.7614\, b\rho\chi\right] \tag{6}$$

$$\frac{k}{k^*} = b\rho\left[\frac{1}{b\rho\chi} + \frac{6}{5} + 0.7574\, b\rho\chi\right] \tag{7}$$

$$\frac{\rho\mathcal{D}}{(\rho\mathcal{D})^*} = \frac{b\rho}{b\rho\chi} \tag{8}$$

where the quantities μ/μ^*, k/k^*, and $(\rho\mathcal{D})/(\rho\mathcal{D})^*$ represent the ratio of the respective transport property at any temperature and pressure to that of the dilute gas at the same temperature. For real gases Enskog suggested that the molulus $b\rho\chi$ be obtained from PVT data using the following relationship:

$$b\rho\chi = \frac{M}{R\rho}\left(\frac{\partial P}{\partial T}\right)_\rho - 1 \tag{9}$$

The parameter χ appearing in the Enskog modulus, $b\rho\chi$, is a factor for the probability of collisions, which for rigid spheres, Boltzmann (2) and Clausius (4) developed the following relationship:

$$\chi = 1 + \frac{5}{8} b\rho + 0.2869 (b\rho)^2 + 0.115 (b\rho)^3 \qquad (10)$$

The PVT information presented in Figures 1 and 2 has been used to establish $b\rho\chi$ values for para-hydrogen. Since this information is presented in terms of reduced quantities, Equation (9) was transformed to express the Enskog modulus in terms of these quantities as follows:

$$b\rho\chi = \frac{Z_c}{\rho_R} \left(\frac{\partial P_R}{\partial T_R} \right)_{\rho_R} - 1 \qquad (11)$$

For para-hydrogen, the critical compressibility factor, $Z_c = 0.3025$.

Reduced pressures and reduced temperatures corresponding to constant reduced densities were obtained from enlarged plots of Figures 1 and 2. These values were used to obtain the P_R versus T_R relationships presented in Figure 8. The isochors of this figure are nearly straight lines and terminate either on the vapor pressure curve or on the solid-liquid line. Each isochor was fitted by a least-squares criterion to a polynomial of third degree or less and the quantity $(\partial P_R / \partial T_R)_{\rho_R}$ was determined by differentiation. This partial derivative was then used to calculate, with Equation (11), the Enskog modulus, $b\rho\chi$. The results of this effort are expressed in the correlation of the Enskog modulus, $b\rho\chi$, presented in Figure 9. This correlation covers the range of the experimental PVT measurements and includes the envelope for the saturated vapor and liquid states. The value of the Enskog modulus at the critical point resulting from this computational procedure is $(b\rho\chi)_c = 0.492$.

In order to apply Equations (6), (7), and (8), advantage is taken of the fact that the value of χ approaches unity, not only for rigid

spheres, but also for real gases, as the ideal gas state is approached. Therefore, at constant temperature, $b\rho\chi/\rho = b\chi$ has the limiting value of b as $\rho \to 0$. In order to deal with a dimensionless quantity, the ratio $b\rho\chi/\rho_R$ has been employed to yield the group $b\rho_c$ as the limiting value. Consequently, for several reduced temperatures, $T_R \geq 1.00$, plots of $b\rho\chi/\rho_R$ versus ρ_R were prepared and extrapolated to $\rho_R = 0$ to establish the intercepts $b\rho_c$. The group $b\rho_c$ was found to be strongly dependent on temperature, and this dependence can be expressed as

$$b\rho_c = \frac{0.667}{T_R^{0.4283}} \tag{12}$$

The resulting values of b and $b\rho\chi$ in conjunction with the PVT data enabled the calculation of the ratios μ/μ^*, k/k^*, and $\rho\mathcal{D}/(\rho\mathcal{D})^*$ as functions of reduced temperature and pressure from Equations (6), (7), and (8). These ratios were obtained for the gaseous and liquid states up to $T_R = 3.0$ and $P_R \approx 30$, including the saturated envelope. Figure 10 presents the μ/μ^* correlation, while Figure 11 presents the k/k^* correlation. For self-diffusivity, a more convenient form which does not require density for its use is the following:

$$\frac{P\mathcal{D}}{(P\mathcal{D})^*} = z\frac{\rho\mathcal{D}}{(\rho\mathcal{D})^*} \tag{13}$$

Consequently, the ratio $P\mathcal{D}/(P\mathcal{D})^* = z/\chi$ was correlated with P_R and T_R to generate the isothermal relationships presented in Figure 12. The correlations presented in Figures 10, 11, and 12 permit the prediction of μ, k, and $\mathcal{D}$ for any temperature and pressure once the corresponding transport property is available for the dilute gaseous state.

The validity of Figure 10 has been checked with the viscosity data of Diller (10). For these comparisons, the viscosity for the dilute gaseous state, μ^*, was obtained from an equation presented by Diller (10). Viscosities for several of his experimental conditions were calculated using

Figure 10 and were compared with corresponding experimental values. The viscosity at the critial point is predicted to be $\mu_c = 36.6 \times 10^{-6}$ g/cm sec as compared to Diller's estimated value of $\mu_c = (35.5 \pm 0.5) \times 10^{-6}$ g/cm sec. For the liquid state, excessive deviations were encountered and therefore it is concluded that the correlation of Figure 10 fails to predict properly the viscosity in this region. The comparisons indicate that the accuracy of prediction is largely dependent on density and not on temperature and pressure. At high densities, the deviations were found to be large and consistently negative. At low densities, the deviations tended to increase and were found to be consistently positive. For the moderate density range, $0.5 < \rho_R < 1.5$, the average absolute deviation was 5.0%.

These comparisons indicate that good agreement can be expected from the use of Figures 10, 11, and 12 for moderate densities. At higher densities, including the liquid state, Enskog's classical approach appears to fail and the more comprehensive model which includes quantum effects is required to account properly for the behavior of this substance in this region.

To improve upon the prediction of the pressure dependence of thermal conductivity as developed from the Enskog theory (12), presented in Figure 11, a novel approach has been employed which utilizes the established viscosity behavior obtained from the experimental measurements of Diller (10). As a point of departure, it is noted that the ratio, $(k/k^*)/(\mu/\mu^*)$, obtained by dividing Equation (7) by Equation (6) becomes a function of $b\rho\chi$ alone. Therefore, the effects of temperature and pressure are included in the parameter $b\rho\chi$. In order to render the dependence of $(k/k^*)/(\mu/\mu^*)$ on $b\rho\chi$ generally applicable to all substances, it is necessary to normalize these quantities. To do this, the reference state has been chosen

to be the critical point. Hence, at the critical point, the ratio, $(k/k^*)/(\mu/\mu^*)$ becomes $(k_c/k^*_{T_c})/(\mu_c/\mu^*_{T_c})$ and the parameter $\rho\chi$ becomes $(\rho\chi)_c$, producing the following normalized quantities

$$R = \frac{(k/k^*)/(\mu/\mu^*)}{(k_c/k^*_{T_c})/(\mu_c/\mu^*_{T_c})} \tag{14}$$

and

$$(\rho\chi)_R = \frac{\rho\chi}{(\rho\chi)_c} \tag{15}$$

The validity of this development hinges on the postulation that the relationship between R and $(\rho\chi)_R$ is general and applicable to all substances. For a reference substance, argon was selected since its PVT, viscosity, and thermal conductivity behavior is well established for the dense gaseous and liquid regions (21,24,25). The dependence of R upon $(\rho\chi)_R$ in the dense gaseous and liquid states is presented in Figure 13. This dependence was not unique as indicated from the Enskog theory, but was found to be a weak function of temperature. The $\rho\chi$ values for para-hydrogen presented in Figure 9, and the viscosities obtained from Figure 6 permitted the establishment of the temperature and pressure dependence of the quantity of $(k/k^*)/(k_c/k^*_{T_c})$ for para-hydrogen. The value $k_c/k^*_{T_c} = 2.37$ for para-hydrogen was obtained from Figure 11. The resulting pressure dependence of thermal conductivity for para-hydrogen, k/k^*, is presented in Figure 14 for the gaseous and liquid states and covers temperatures up to $T_R = 3.0$ and pressures up to $P_R = 30$.

Since the difference between the thermal conductivity of para-hydrogen and normal hydrogen in the dilute gaseous state is negligible (11), the data for normal hydrogen from seven sources have been analyzed to yield the relationship

$$k^* = [0.1674T - 0.000059T^2] \times 10^{-5} \tag{16}$$

where T is in degrees Kelvin.

Figure 14 and Equation (16) offer a means for establishing preliminary thermal conductivities for para-hydrogen in the gaseous and liquid states, and until such a time when dependable experimental values become available, their use is recommended.

NOMENCLATURE

b	Enskog factor for molecular volume, cm^3/g
H	absolute enthalpy, Btu/lb
H_o°	absolute enthalpy at $T=0°K$
k	thermal conductivity, cal/sec cm °K
k^*	thermal conductivity of dilute gas, cal/sec cm °K
k_c	thermal conductivity at critical point, cal/sec cm °K
$k^*_{T_c}$	thermal conductivity of dilute gas at critical temperature, cal/sec cm °K
M	molecular weight
P	pressure, atm
P_c	critical pressure, atm
P_R	reduced pressure, P/P_c
P_t	vapor pressure at triple point, mm Hg
R	gas constant
R	thermal conductivity - viscosity parameter, Equation (13)
S	absolute entropy, Btu/lb °R
T	temperature, °K
T_b	normal boiling point, °K
T_c	critical temperature, °K
T_R	reduced temperature, T/T_c
T_t	triple point temperature, °K
v	molar volume, cm^3/g-mole

v_c critical volume, $cm^3/g\text{-mole}$

z compressibility factor, Pv/RT

z_c critical compressibility factor, $P_c v_c / RT_c$

Greek Letters

$\mathfrak{D}$ self-diffusivity, cm^2/sec

$\mathfrak{D}^*$ self-diffusivity of dilute gas, cm^2/sec

μ viscosity, $g/sec\ cm$

μ^* viscosity of dilute gas, $g/sec\ cm$

μ_c viscosity at critical point, $g/sec\ cm$

μ_H^* viscosity of normal hydrogen in the dilute gaseous state, $g/sec\ cm$

μ_P^* viscosity of para-hydrogen in the dilute gaseous state, $g/sec\ cm$

μ_R reduced viscosity, μ/μ_c

$\mu_{T_c}^*$ viscosity of dilute gas at critical temperature, $g/sec\ cm$

ρ density, g/cm^3

ρ^* density of dilute gas, g/cm^3

ρ_c critical density, g/cm^3

ρ_R reduced density, ρ/ρ_c

χ Enskog factor for probability of collisions

LITERATURE CITED

1. Barber, C. R. and A. Horsford, Brit. J. Appl. Phys. 14, 920 (1963).
2. Boltzmann, Ludwig, Amsterdam, Ak. Proc. 1, 403 (1899).
3. Brebach, W. J. and George Thodos, Ind. Eng. Chem. 50, 1095 (1958).
4. Clausius, R. J. E., "Mechanische Wärmetheorie," 3, 57, F. Vieweg und Sohn, Braunschweig (1889).
5. Clusius, K. and K. Hiller, Z. physik. Chem. (Leipzig) B4, 158 (1929).

6. Coremans, J. M. J., A. Van Itterbeek, J. J. M. Beenakker, H. F. P. Knapp, and P. Zandbergen, Physica 24, 557 (1958).

7. De Palma, J. V., M. S. thesis, Northwestern University, Evanston, Illinois (1965).

8. De Palma, J. V. and George Thodos, J. Spacecraft and Rockets 3, 747 (1966).

9. De Palma, J. V. and George Thodos, J. Chem. Eng. Data 11, 31 (1966).

10. Diller, D. E., J. Chem. Phys. 42, 2089 (1965).

11. Elzinga, D. J. and George Thodos, "Predicted Thermal Conductivities for Para-Hydrogen in the Dense Gaseous and Liquid States," to be submitted for publication.

12. Enskog, David, Svensk. Akad. Handl. 63, No. 4 (1922).

13. Frost, A. A. and D. R. Kalkwarf, J. Chem. Phys. 21, 264 (1953).

14. Goodwin, R. D., D. E. Diller, H. M. Roder, and L. A. Weber, J. Research Natl. Bur. Standards 67A, 173 (1963).

15. Goodwin, R. D. and H. M. Roder, Cryogenics 3, 12 (1963).

16. Hoge, H. J. and R. D. Arnold, J. Research Natl. Bur. Standards 47, 63 (1951).

17. Johnston, H. L., T. J. Clarke, E. B. Rifkin, and E. C. Kerr, J. Am. Chem. Soc. 72, 3933 (1950).

18. Kennedy, J. T. and George Thodos, A.I.Ch.E. Journal 7, 625 (1961).

19. Kobe, K. A. and R. E. Lynn, Jr., Chem. Revs. 52, 117 (1953).

20. Mendelssohn, K., M. Ruhemann, and F. Simon, Z. physik. Chem. (Leipzig) B15, 121 (1931).

21. Owens, E. J. and George Thodos, A.I.Ch.E. Journal 3, 454 (1957).

22. Roder, H. M., D. E. Diller, L. A. Weber, and R. D. Goodwin, Cryogenics 3, 16 (1963).

23. Roder, H. M., L. A. Weber, and R. D. Goodwin, National Bureau of Standards Monograph 94 (1965).

24. Rosenbaum, B. M., Steven Oshen, and George Thodos, J. Chem. Phys. 44, 2831 (1966).

25. Shimotake, Hiroshi and George Thodos, A.I.Ch.E. Journal 4, 257 (1958).

26. Stiel, L. I. and George Thodos, Ind. Eng. Chem. (Fundamentals) 2, 233, (1963).

27. Vanderslice, J.T., Stanley Weissman, E. A. Mason and R. J. Fallon, Phys. Fluids 5, 155 (1962).

28. Weber, L. A., D. E. Diller, H. M. Roder, and R. D. Goodwin, Cryogenics 2, 236 (1962).

29. Wooley, H. W., R. B. Scott, and F. G. Brickwedde, J. Research Natl. Bur. Standards 41, 379 (1948).

30. Younglove, B. A., and D. E. Diller, Cryogenics 2, 283 (1962).

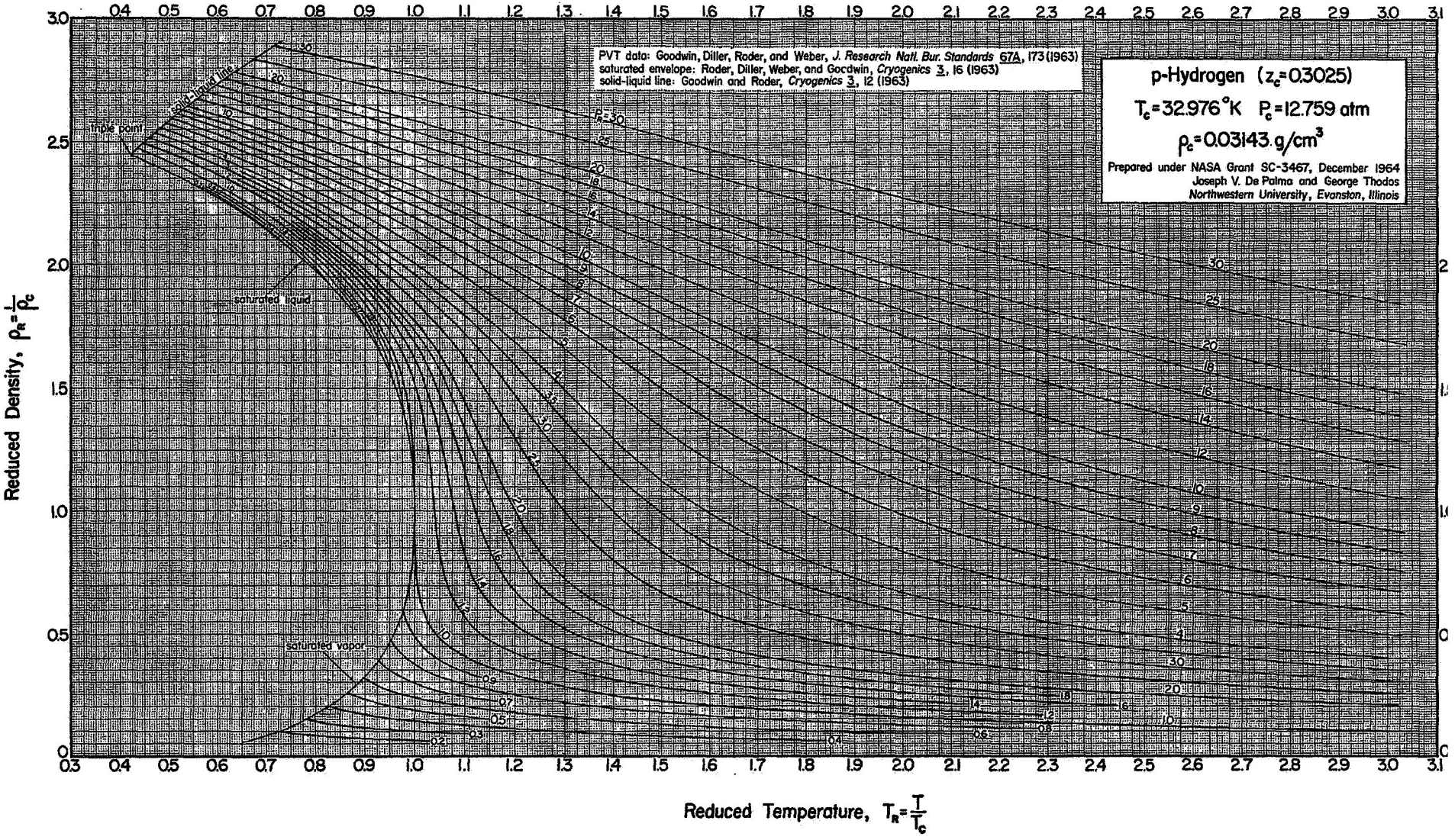

Figure 1. Reduced density correlation for p-hydrogen
(rectilinear coordinates)

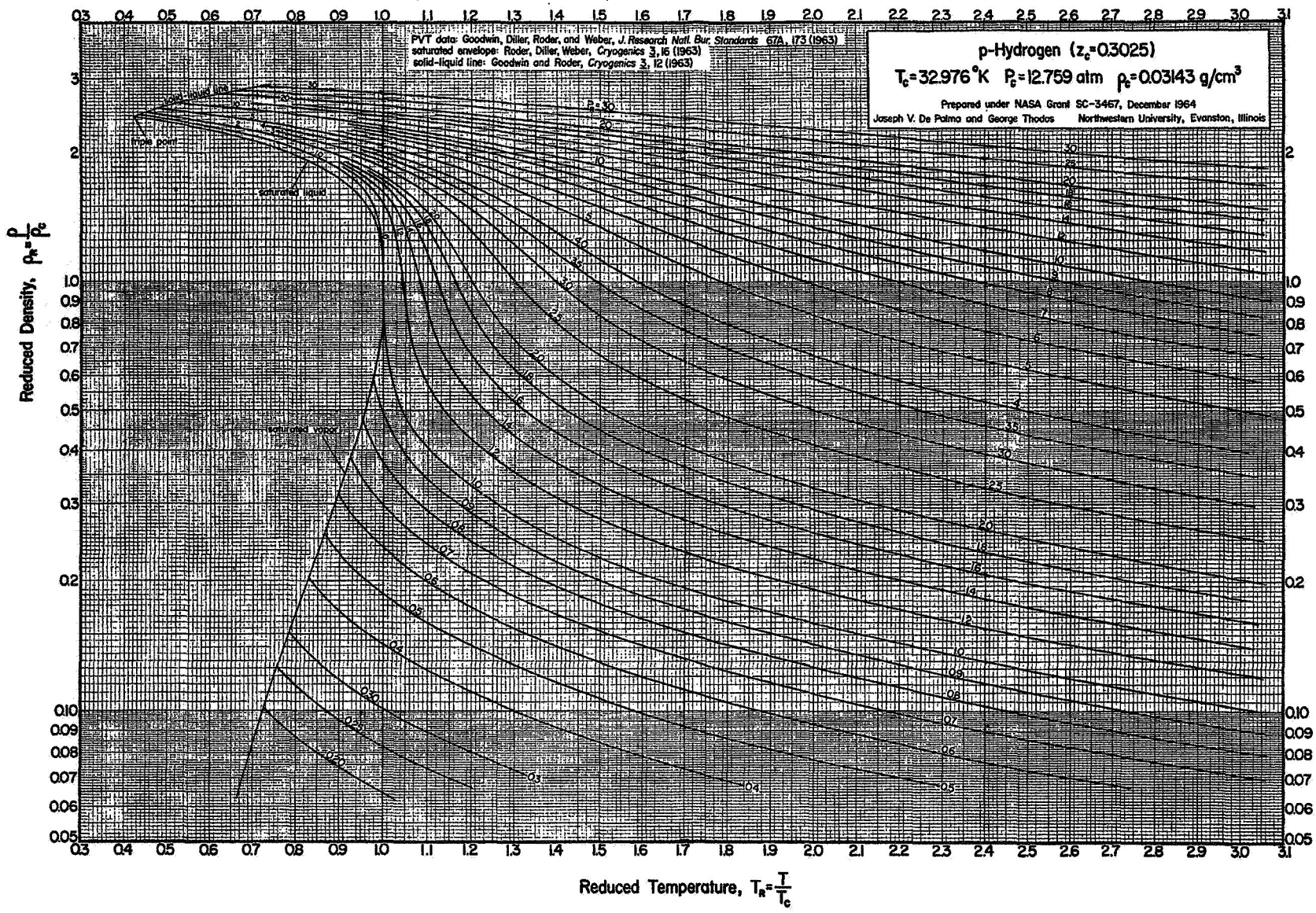

Figure 2. Reduced density correlation for p-hydrogen
(semi-log coordinates)

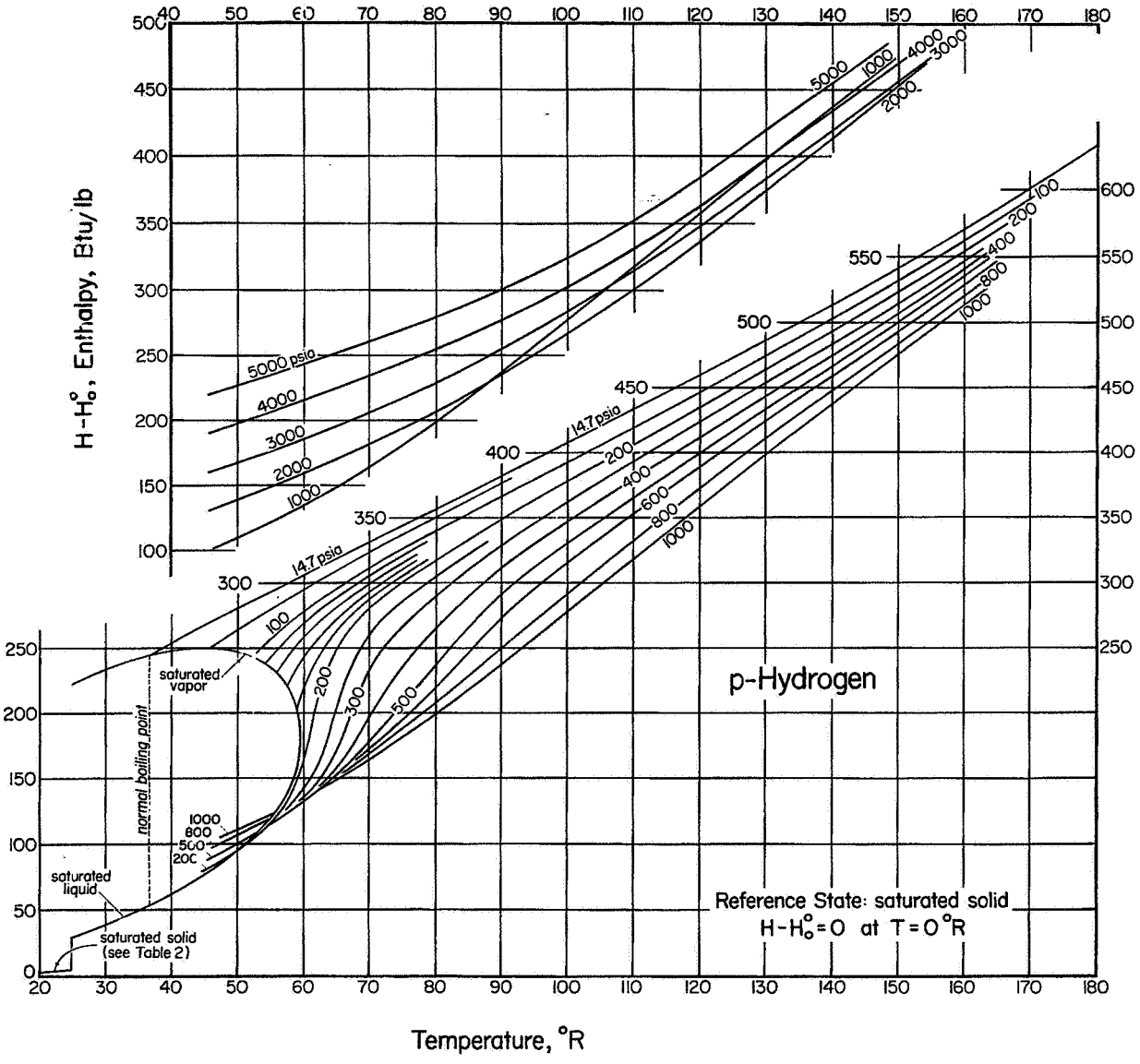

Figure 3. Enthalpy diagram for p-hydrogen

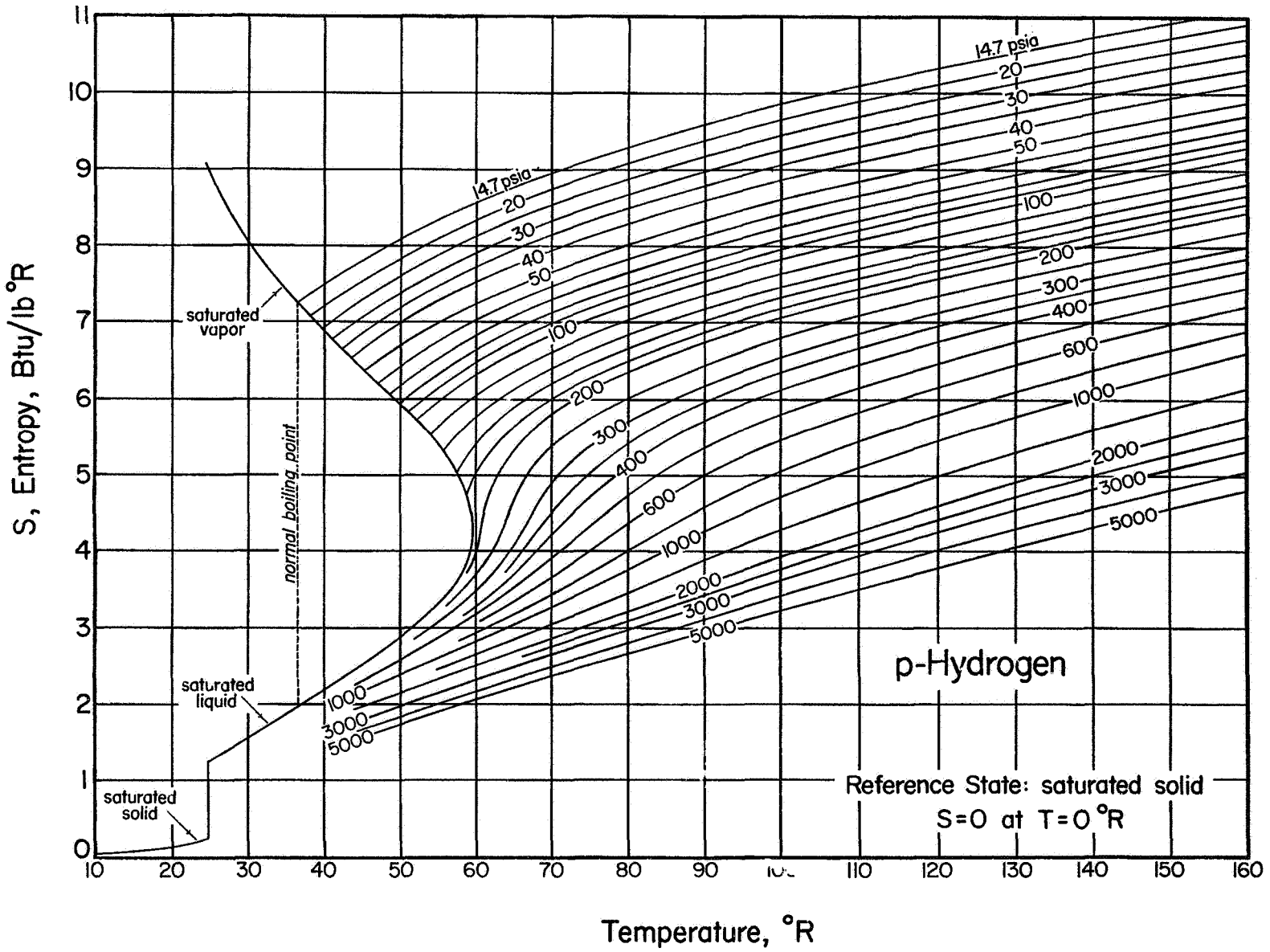

Figure 4. Entropy diagram for p-hydrogen

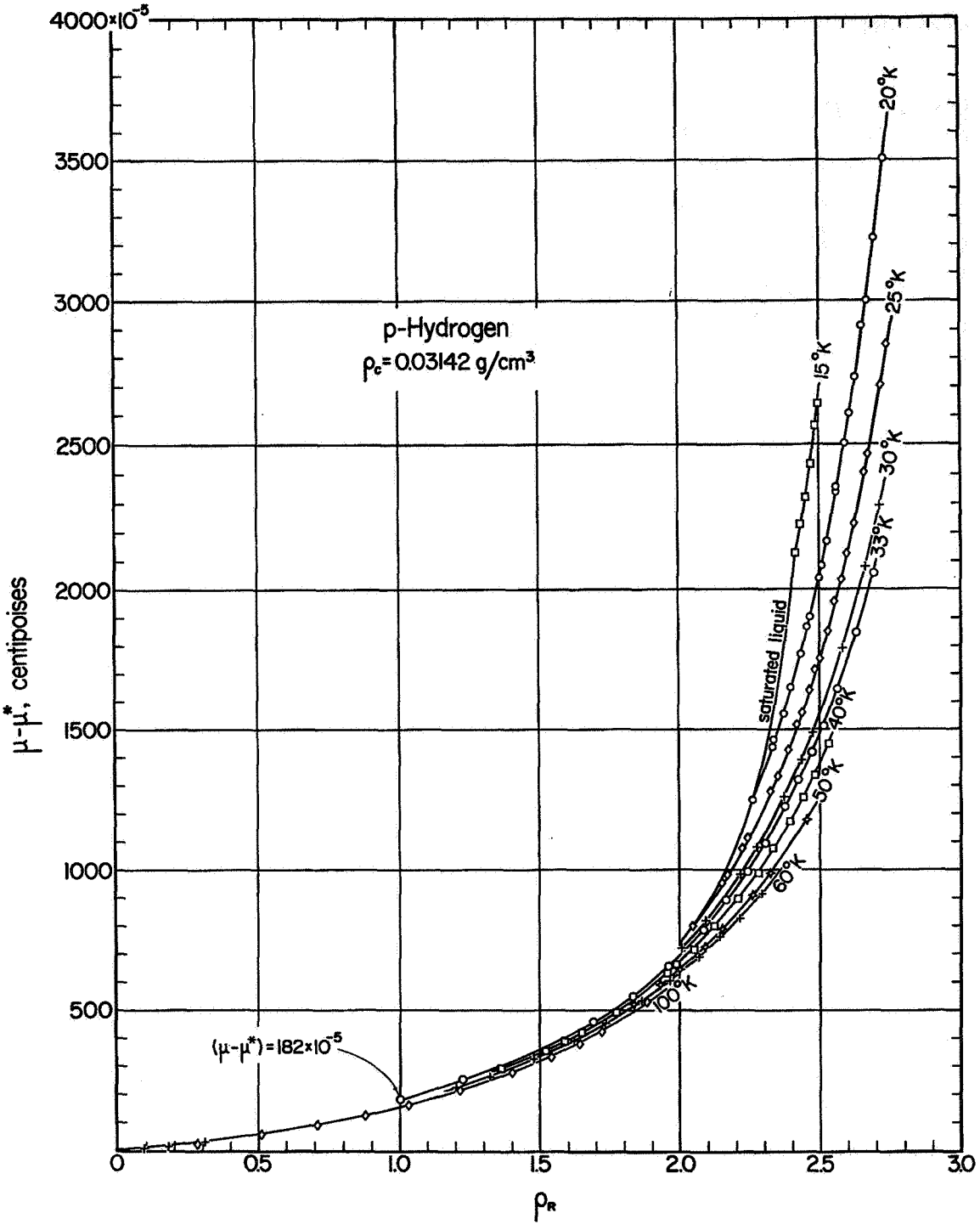

Figure 5. Constant temperature relationships between $\mu-\mu^*$ and ρ_R for the gaseous and liquid states of para-hydrogen

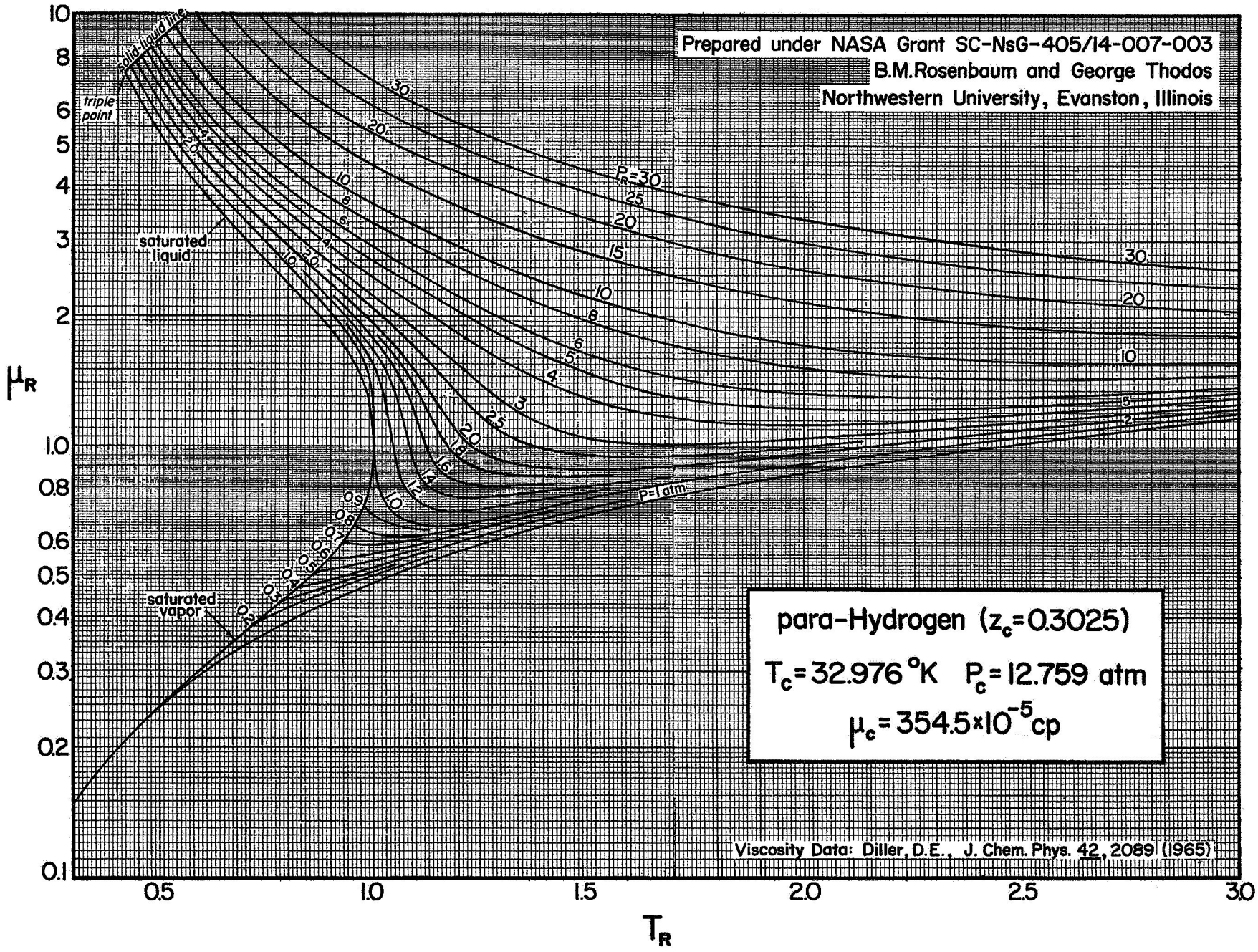

Figure 6. Reduced viscosity correlation for para-hydrogen in the gaseous and liquid states at cryogenic temperatures

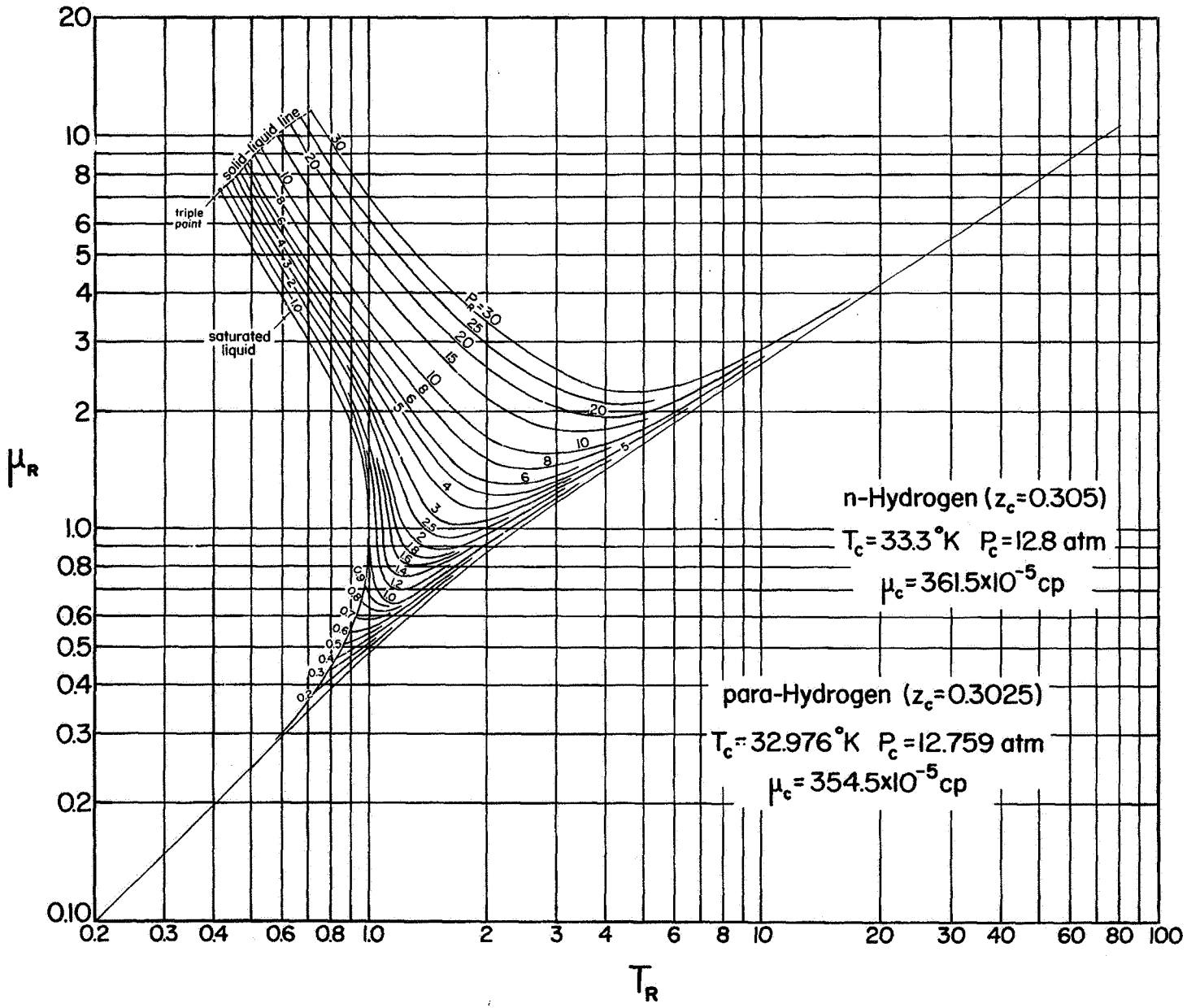

Figure 7. Reduced viscosity correlation for normal and para-hydrogen in the gaseous and liquid states

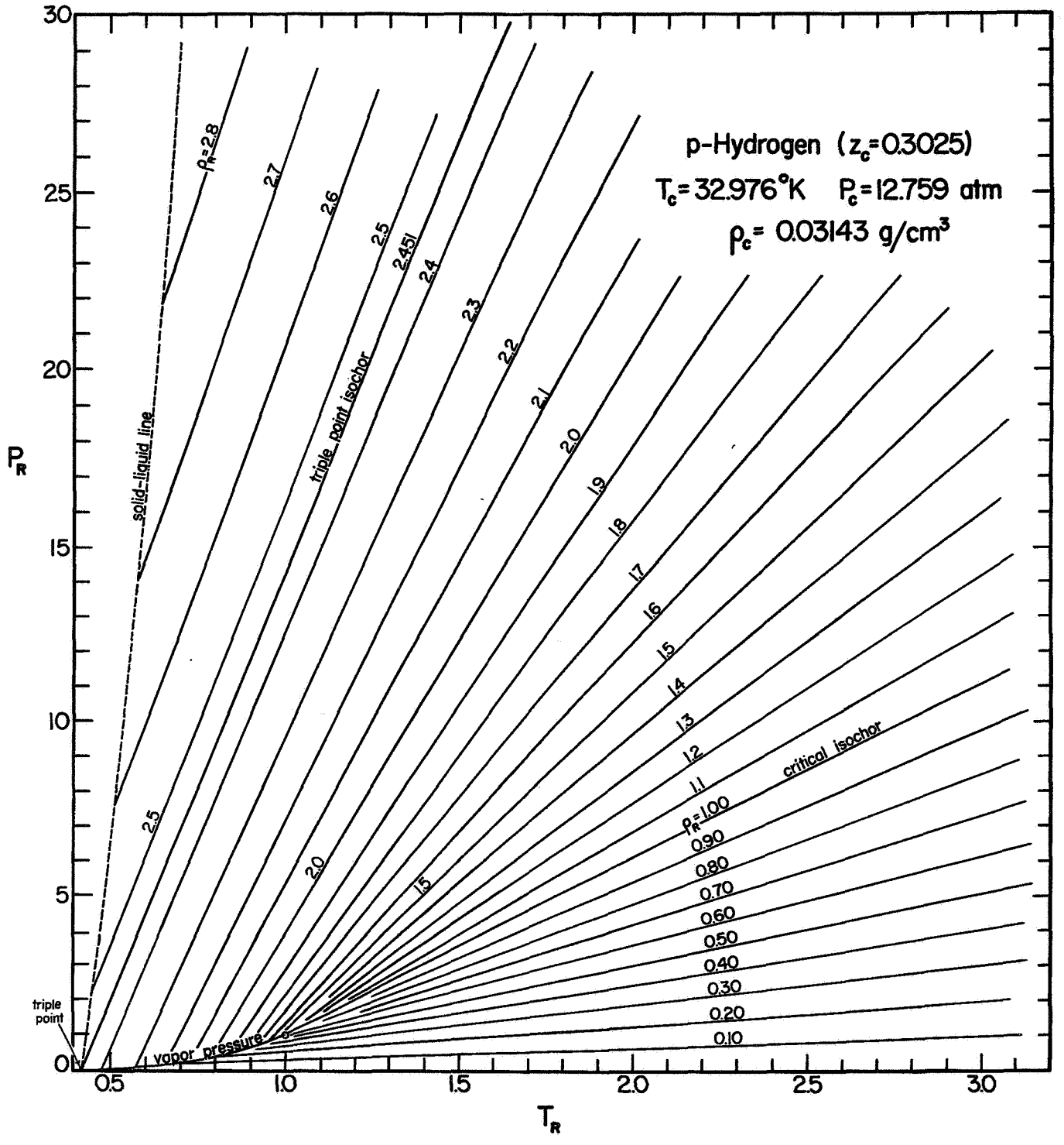

Figure 8. Relationships between P_R and T_R for p-hydrogen at constant reduced densities, ρ_R

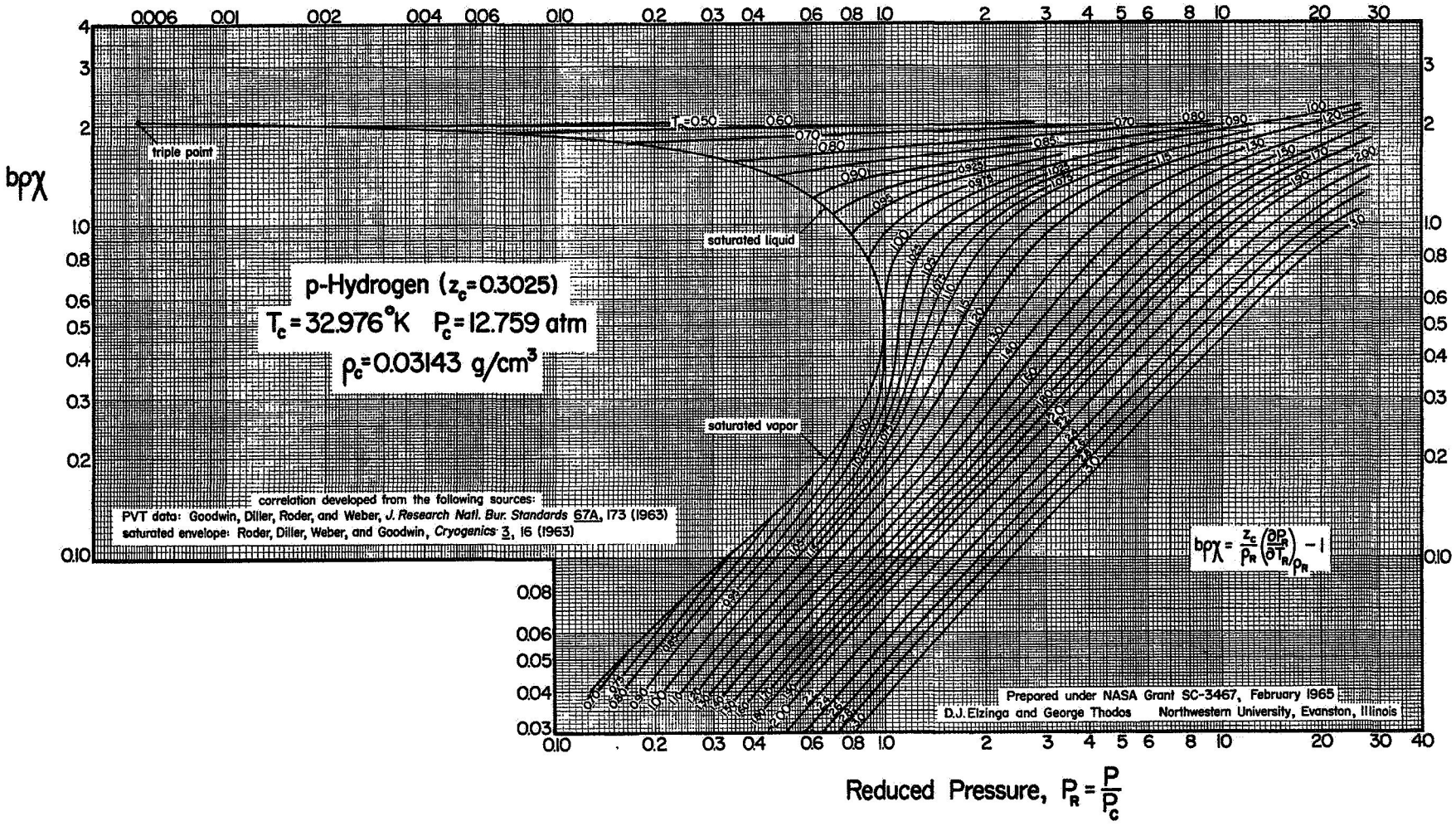

Figure 9. Correlation of the Enskog modulus, $b\rho\chi$, with reduced temperature and pressure for p-hydrogen

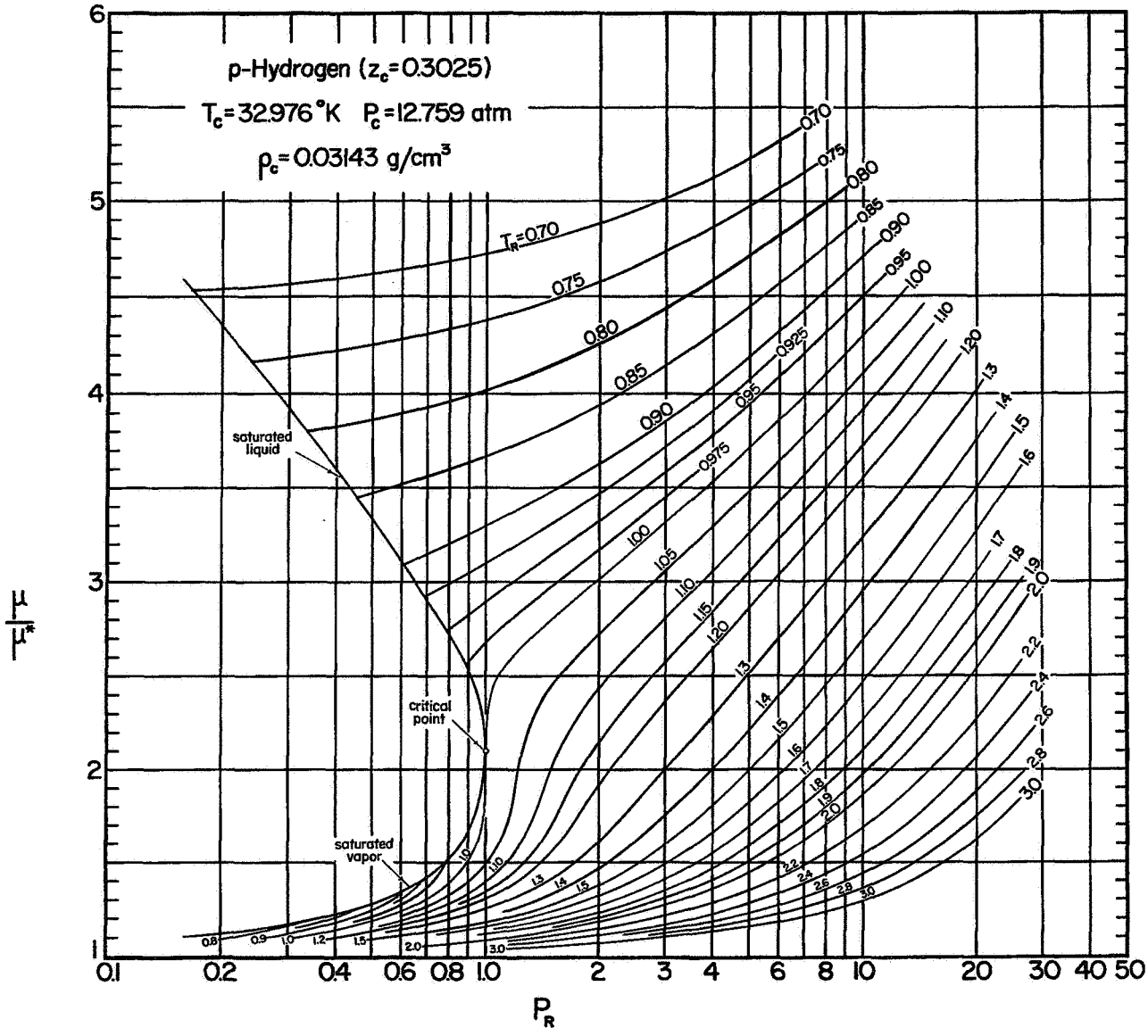

Figure 10. Correlation between μ/μ^*, P_R, and T_R for p-hydrogen (calculated from Enskog theory)

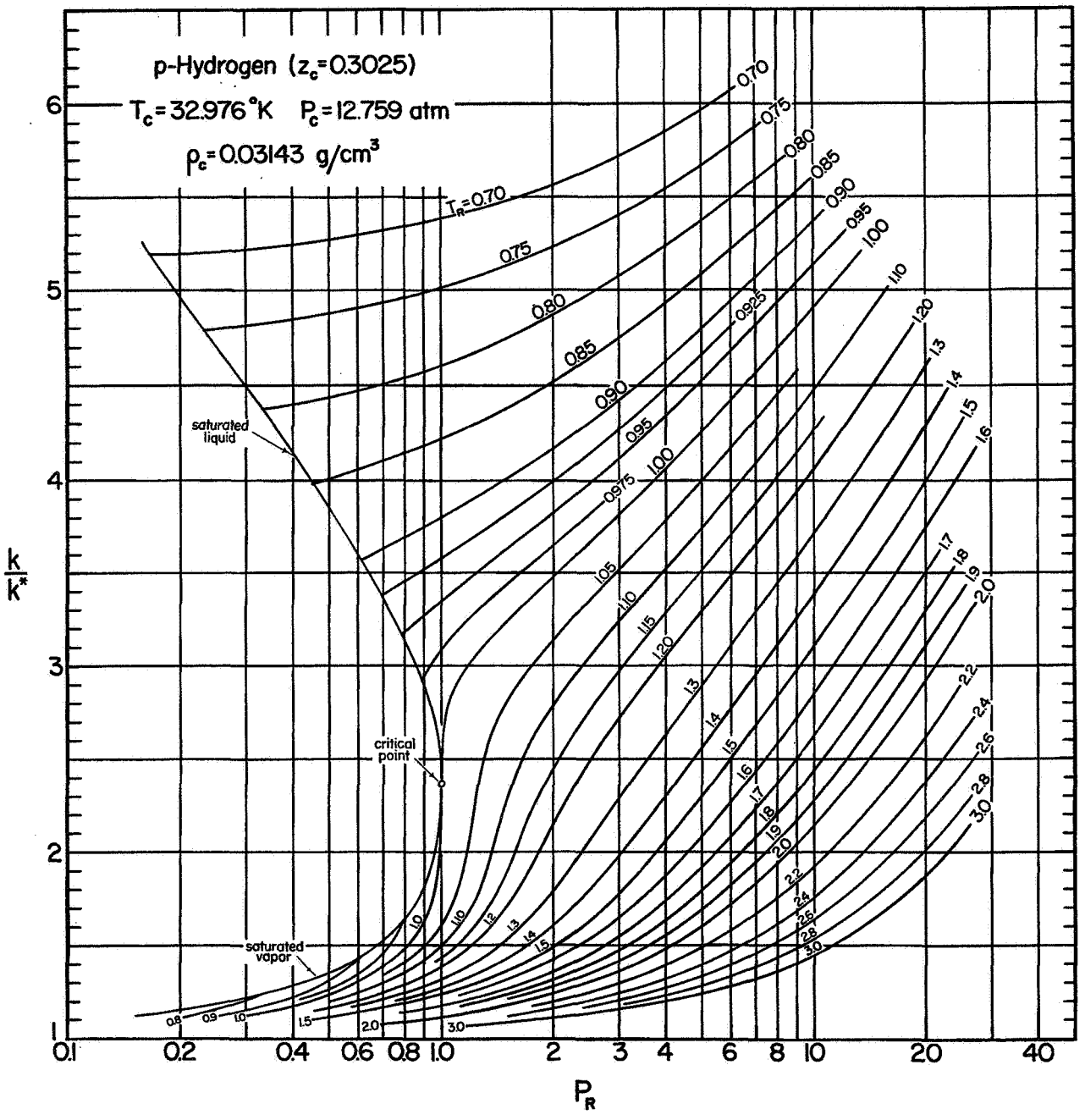

Figure 11. Correlation between k/k^*, P_R, and T_R for p-hydrogen (calculated from Enskog theory)

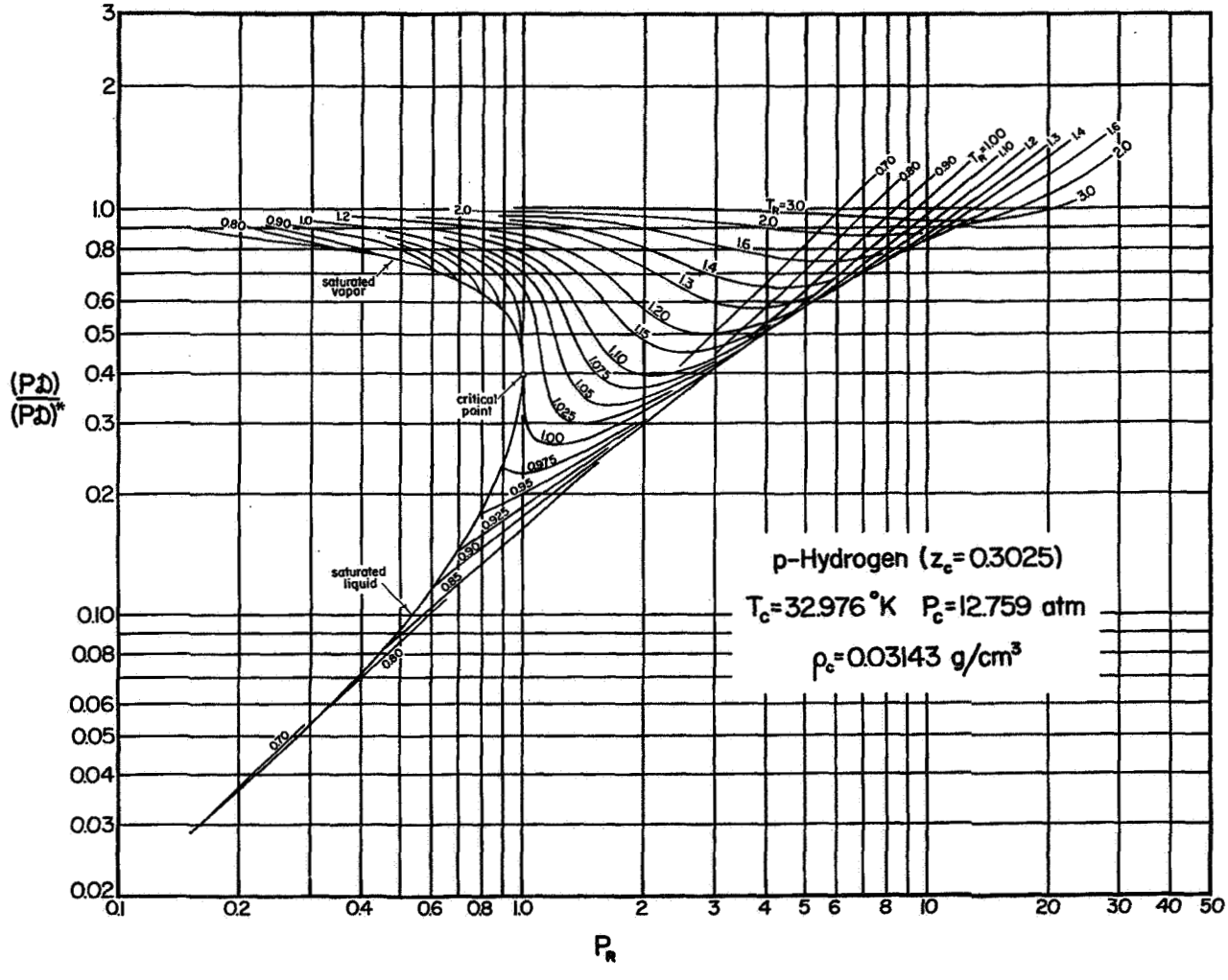

Figure 12. Correlation between $(PD)/(PD)^*$, P_R, and T_R for p-hydrogen (calculated from Enskog theory)

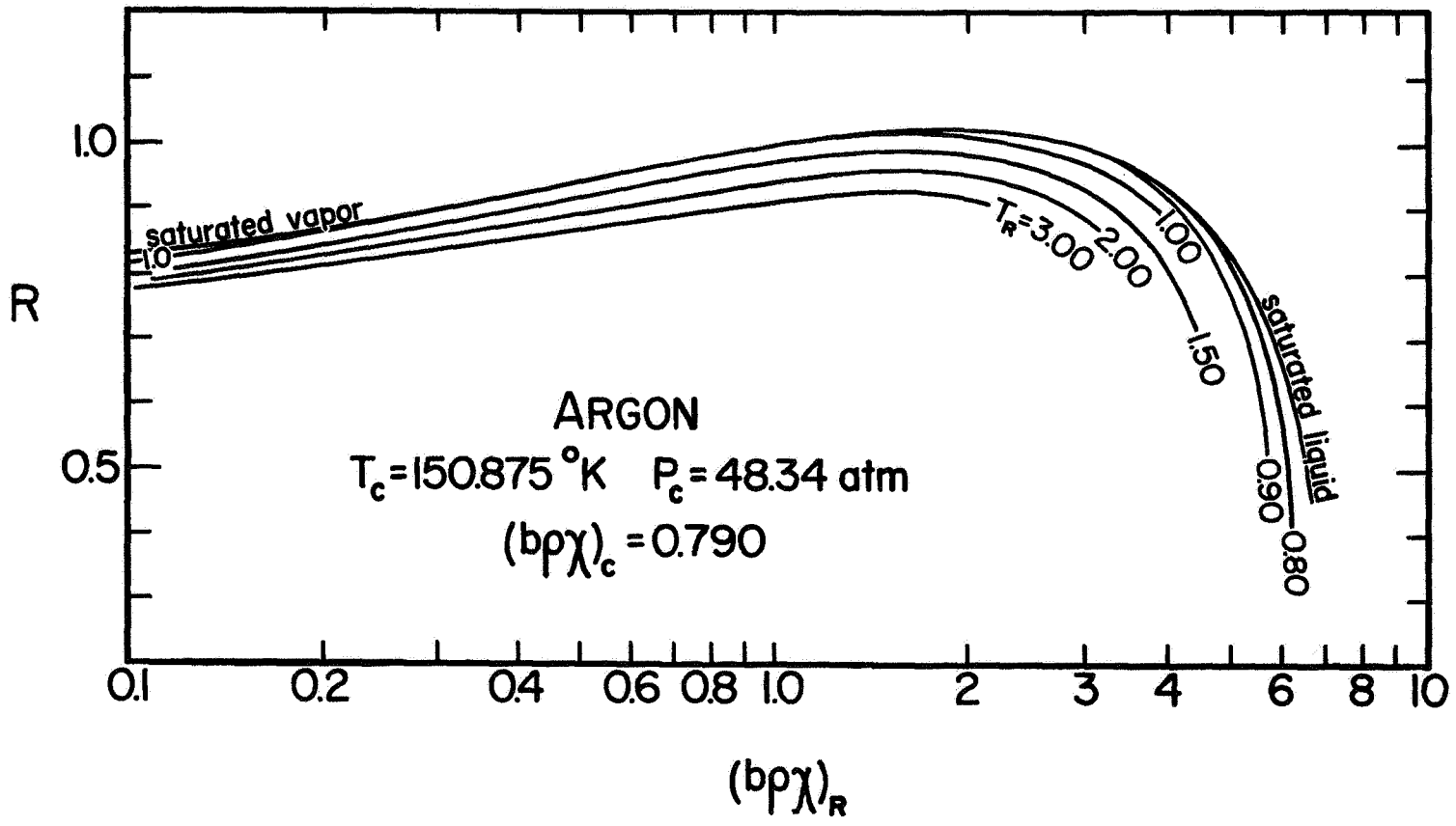

Figure 13. Generalized relationships between R and $(b\rho\chi)_R$ based on argon

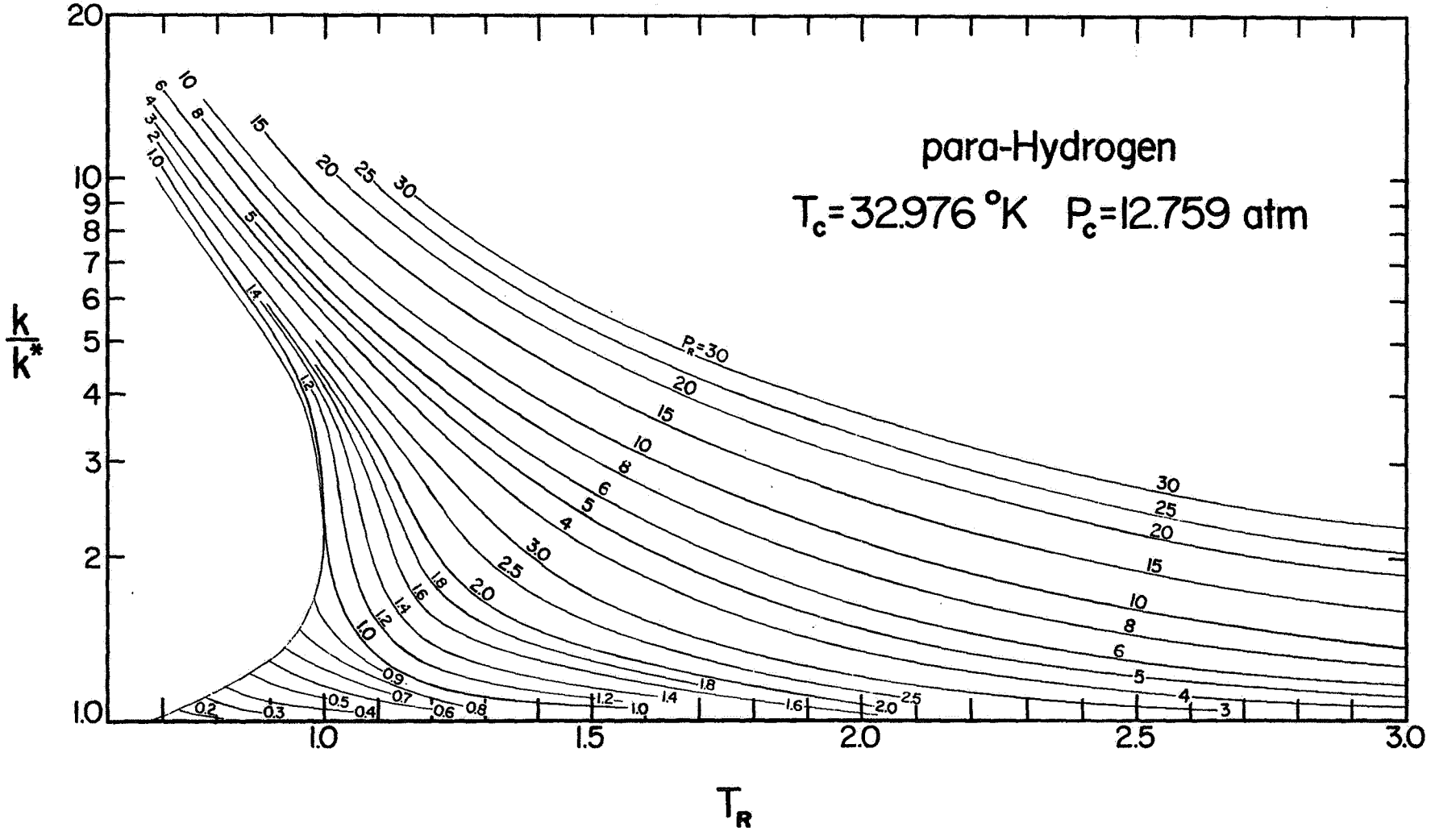

Figure 14. Predicted pressure dependence of thermal conductivity for para-hydrogen in the gaseous and liquid states